Final accepted version of
Bakker, M., Antoniazza, G., Odermatt, M. and Lane, S.N., 2019. Morphological response of an Alpine braided reach to sediment-laden flow events. Journal of Geophysical Research – Earth Surface, 124, 1310-28
Published version available at:https://agupubs.onlinelibrary.wiley.com/doi/abs/10.1029/2018JF004811

Morphological Response of an Alpine Braided Reach to Sediment-Laden Flow Events

M. Bakker[1*], G. Antoniazza[1], E. Odermatt[1] and S.N. Lane[1]

[1]Institute of Earth Surface Dynamics, University of Lausanne, Switzerland.

[*]currently at ETNA, Irstea, University Grenoble Alpes, France.

Corresponding author: Maarten Bakker (maartenbakker@yahoo.com)

Key Points:

- Braided river response to long-duration floods shows the effects of local relief, filling of lows and erosion of highs
- Morphodynamic response to short and abrupt sediment-laden flows reveals system memory with alternating local erosion and sedimentation
- The internal morphodynamics of a braided river condition their own response to upstream flow events and thus downstream sediment transfer

Abstract

Braided gravel-bed rivers show characteristic temporal and spatial variability in morphological change and bedload transport under steady flow and sediment supply rates. Their morphodynamic behavior and long-term evolution in response to non-stationary external forcing is less well known. We studied daily morphological changes in a well-constrained reach of an Alpine braided river that is subject to regulated sediment-laden flows, associated with hydro-electric power exploitation, as well as occasional floods. We found that net reach erosion and deposition were forced by upstream sediment supply, albeit in a non-linear fashion. The spatial distribution of morphological change and inferred spatially-distributed sediment transport rates varied strongly along the braided reach and between successive sequences of flushing. Local morphological change was driven by two factors: 1) local relief, leading to the preferential filling of topographic lows and erosion of highs, particularly during longer duration floods, which allow braided dynamics to be maintained; and 2) system memory, leading to a negative autocorrelation in bed level changes where erosion was followed by deposition of similar magnitude and vice versa. This effect was associated with the temporary storage of high sediment loads from flushing due to the abrupt on-off nature of these flows, and reveals the relatively efficient transport of sediment in a river that is heavily impacted upon by flow abstraction. In general, the internal morphodynamics of the braided river condition their own response to external forcing events and thus sediment transfer.

1 Introduction

Braided river reaches form an important link in the storage and transfer of sediment in Alpine systems. Their beds can accommodate and release large amounts of sediment through erosion and deposition within channel and bar complexes (Ashmore, 1991; Ferguson, 1993). The result is high spatial and temporal variability in sediment storage and associated sediment transport across multiple scales (Hoey, 1992). It is therefore crucial to understand the internal functioning of braided river reaches if we want to gain insight into their response to external forcing mechanisms including high-magnitude flow events (e.g. Bertoldi et al., 2010; Warburton, 1994), climate change and flow management (e.g. Lane et al. 2017).

The complexity of braided gravel-bed streams has long been investigated in controlled flume experiments where cyclical variability in bedload transport was found at various temporal and spatial scales (e.g. Gomez et al. 1989) and bed morphology (e.g. Ashmore 1982). These experiments have shown braiding can occur under steady flow and sediment supply rates, and it is therefore a fundamental instability autogenically arising from the interaction between flowing water and a mobile bed, provided river banks remain erodible (Murray & Paola, 1994). In natural systems, the actual functioning of braided gravel-bed streams may be more complex because they respond to and evolve with changing upstream conditions (Lane et al. 1996) over a wide range of spatial and temporal scales. This is particularly the case in Alpine mountain streams that are typically subject to large temporal fluctuations in both flow and sediment supply (quantity and caliber). In addition, there may be time-dependent feedback mechanisms associated with the legacy of events themselves or processes operating between events. For instance, the deposition associated with one event may provide ample sediment supply for the next, while, on the other hand, low flows between events may lead to bed surface stabilization (e.g. Reid et al., 1985; Turowski et al., 2011) and affect the ease of sediment entrainment. We refer to these as memory effects. Thus, the combination of fundamental instabilities in braiding, continuously evolving upstream forcing and memory effects in system response make it difficult to unravel the nature of braided river morphodynamics and the underlying driving processes.

In this study, we investigated the morphodynamics of a well-constrained Alpine braided river reach, the Borgne d'Arolla in Switzerland. The reach is more or less dry for most of the time due to flow intake and diversion for hydroelectric power (hydropower) generation, with the exception of frequent sediment-laden flows which are used to flush sediment from flow intakes and occasional, non-regulated floods (Bakker et al., 2018). Our aim is to quantify the effect of these flow events and to assess the spatio-temporal extent to which they affect the braided river reach morphodynamics. To accomplish this, we combined event-based flow and sediment records (Bezinge et al., 1989) with high-frequency remote sensing (e.g. Milan et al., 2007; Williams et al., 2013). These data allowed us to characterize changes in river bed morphology and relate these to upstream flow and sediment supply drivers. In addition we could assess spatial patterns in downstream bedload transfer from morphological change using the 2D morphological method (Antoniazza et al., 2019). We will show that this approach gives insight into the spatial structure of braided river bed morphodynamics and, in particular, the distinct morphodynamic signature and sediment transfer associated with flow events and sediment supply in this system.

2 Study Area

The Borgne is a left bank tributary of the Rhône River that drains glaciated basins of the Pennine Alps in south-west Switzerland. In this study, we investigated the 1.7 km long braided headwater reach of the Borgne d'Arolla (Figure 1), whose upstream end lies c. 1 km downstream from the terminus of the Bas Glacier d'Arolla.

Nearly all of the water (c. 90%) from the glacier and upstream tributaries is intercepted by the Lower Bertol intake (Bakker et al., 2018), 225 m from the upstream end of the reach. The intake is one of 75 intakes that make up a wider hydropower scheme that diverts water from the Matter and Hérens valleys via 100 km of pipes and 4 pumping stations to the Lac de Dix reservoir in the Hérémence valley (Park, 1980). Sediment delivered to the intake is trapped in a gravel and subsequent sand traps, which are flushed (also referred to as purged) when they are full, i.e. water abstraction is temporarily stopped (for typically 15-30 minutes) and flow is used to evacuate sediment from the traps into the braided reach (Bezinge et al., 1989; Gurnell et al., 1988). There are two important exceptions to this (semi-)automatic operation which are related to the flow management of the hydropower system. First, precautionary night-time flushing events (starting at midnight with an approximate duration of 1 hour) are performed for safety and sediment transfer purposes when the sediment trap is at least half full (Bakker et al., 2018). In this case longer duration flushing is designed to coincide with flushing of upstream intakes, most notably the Haut Glacier d'Arolla intake (Lane et al., 2017). Second, under exceptionally high flow conditions, that typically occur during very warm days in the (late) summer, water cannot always be abstracted due to the limited capacity of the flow transfer system and water intake is stopped at the Lower Bertol intake to prevent system overload. These events and in particular the long duration floods in combination with flushing of upstream intakes, have a strong impact on morphological change in the investigated reach (Bakker et al., 2018; Gurnell, 1983).

Table 1 shows the dimensions of and general hydraulic parameters for the braided reach. Nearly all sediment that is supplied to the reach comes from Lower Bertol intake flushing (and flood) events. There are a few small, unregulated tributaries that enter the reach and two regulated (flow abstraction) tributaries: Douves Blanches, which enters the reach on the right bank and is very rarely active (intake data indicate that during 2015, it supplied less than 1% of the total sediment supplied to the reach; Micheletti & Lane, 2016); and Pièce, which has a higher sediment supply (nearly 10% of the total sediment supply), but enters the reach almost at its downstream end on the left bank (see Figure 1).

3 Methods

3.1 Overview

To study morphological change and sediment transport in the braided reach we benefit from the presence of flow abstraction in two ways. First, we used intake data provided by the hydropower company Grande Dixence SA to determine discharge and, indirectly through identifying flushing events, to estimate the sediment supply to the reach during flow events (Bakker et al., 2018). Second, because the riverbed is more or less dry between flushing events, we were able to use a terrestrial laser scanner to survey the entire river bed topography and to quantify morphological change on a daily basis. We then combined upstream sediment supply and morphological change data to determine reach-based sediment budgets and to infer spatially-distributed mean bedload transport rates, using a routing scheme based on 2D hydraulic flow simulations taking into consideration topographic forcing, in a two-dimensional application of the Exner equation (Antoniazza et al., 2019). Finally, we analyzed the spatial distribution and temporal dynamics of morphological change and sediment transport as a function of upstream forcing, flow and sediment input, river bed morphology and preceding morphological change.

3.2 Flow events: upstream discharge and sediment supply

Fieldwork was performed in the exceptionally warm summer of 2015. The average temperature in July at Sion (where the Borgne enters the Rhône) was 24 °C, 0.7 °C warmer than the previous recorded maximum (MeteoSuisse measurements since the year 1864). The warm conditions led to generally high flow conditions and sediment loads that were observed during frequent flushing events, typically 3 to 6 per day, and 3 longer flood events related to (near) system capacity limitations on 24 July (evening), 10 August (morning) and 14 August (morning).

Daily laser scanner surveys of the braided river reach were performed between 27 July and 13 August, with the exception of 1 and 9 August. In addition, surveys were performed on 6 June and 2 September to capture the long-term change in river bed topography. For the whole period, river flow data were derived based on the identification of distinct flow events from 1-minute flow intake records provided by Grande Dixence SA, accounting for potential flow contribution from the upstream Haut Glacier d'Arolla intake (Bakker et al., 2018); see Figure 2a and 2b. Based on the characteristic timing and estimated water yield of different types of events, we could attribute sediment loads to flushing events that correspond to the full storage capacity of the sand trap, 8 m^3, and gravel trap, 150 m^3, and the estimated storage of the gravel trap during precautionary night-time flushing events, 120 ± 20 m^3 (Figure 2c). Although the long duration floods are inherently uncertain due to their non-regulated nature and continuous throughput of sediment, we attributed a load of 600 m^3 to close the long-term sediment budget.

The obtained flow and sediment yield for the investigation period is given in Figure 2d and for full details on the approach we refer to Bakker et al. (2018).

3.3 Morphological change

3.3.1 Lidar point cloud acquisition

We used a Riegl VZ 6000 terrestrial laser scanner (or lidar) to survey the braided river reach. The scans were taken from a well-accessible vantage point, at an elevation of approximately 2170 m, on the valley slope just above the village of Arolla. This site is in line with the braided reach at a distance of 1200 m from the bridge at the downstream end of the reach (Figure 1 - photo insert). We acquired a 10 to 30 cm resolution point cloud, depending on distance, with a scan time of approximately 7 minutes. The used survey setup is the same as that used by Antoniazza et al. (2019).

We processed the obtained point clouds with Riscan PRO software and registered them to a reference scan (27 July). Here, we adopted the same general procedure as Antoniazza et al. (2019) following Gabbud et al. (2015), based upon: (1) the removal of erroneous points, due to atmospheric reflection and power lines that cross the river; (2) manual coarse registration using fixed points including buildings, (hydropower) infrastructure and stationary boulders; and (3) the application of automatic multi-station adjustment to optimize the alignment of so-called plane patches that were generated from the points clouds (Riegl, 2015) using an inverse distance weighting algorithm (Zhang, 1994). The alignment was based on the area surrounding the river channel, which is assumed to be stable on the timescale of the surveys.

3.3.2 DEM generation

From the point cloud data, we generated 0.2 m resolution Digital Elevation Models (DEMs) (e.g. see the hillshade in Figure 1a). We did this using linear point kriging (with slope and anisotropy equal to 1) in Surfer 10 software. Heritage et al. (2009) found that this interpolation method gave the best results in a comparable setting, using aerial lidar to map a gravel bar.

To quantify the local uncertainty due to interpolation, we evaluated the spatial distribution of lidar point density (Figure 1b). This allows us to directly address the source of the uncertainty, as opposed to combining factors including distance from scanner, aspect of the surface, reflectance of the surface etc. through a fuzzy inference system as proposed by Wheaton et al. (2013) and adopted by Antoniazza et al. (2019). The uncertainty associated with the point density was assessed using a sub-area (size 50 x 50 m) with a high point density, i.e. negligible occlusions and at a relative short distance from the lidar (1400 m distance in Figure 1). We computed a reference DEM at 2.2 m resolution, reflecting the general scale of morphological features in the river and limiting the number of cells with no points. For the same sub-area we computed DEMs with lower point densities (ρ_p) through consecutively removing random points (see Supporting Information S1). This allowed the quantification of the standard deviation of error (σ_E) of these DEMs with respect to the reference grid as a function of point density. We found a clear logarithmic trend with the point density (p value < 0.001, $R^2 = 0.99$) which is described by [1]:

$$\sigma_E = 10^{a \cdot \rho_p + b} \pm c \qquad [1]$$

where a = -0.08 and b = -1.3 were derived from the regression. This trend was consistent for different DEM resolutions and DEMs obtained on different dates (see Supporting Information S1). Additionally c = ±0.02 m was added to the local error function to represent the inherent uncertainty in the equipment itself.

3.3.3 Change detection

To verify residual systematic error in the lidar registration, DEMs of Differences (DoDs) were generated for all dates with respect to the reference date, 27 July (Figure 3a). This revealed residual systematic error, visible as banding in the direction of the laser beams that diverge with increased distance from the laser scanner (for illustration purposes we chose an example with relatively large error). We attribute this error to the instrument operation, potentially related to the mechanics of instrument components which set the vertical angle and which becomes evident at the long range used here. The result is that the error may vary with the horizontal scanning angle and significant changes may occur between scan lines. To correct for this error we assessed changes smaller than 0.20 m, with respect to the reference date for both the river bed and banks. This limit was chosen to account for the largest systematic errors, whilst minimizing the inclusion of actual morphological change, although this cannot be entirely excluded. We applied linear regression to these changes along the distance axis from the lidar (x-axis) for 2.2 m wide bands in the y-axis. The regression function was then used to generate a correction grid (Figure 3b; note the error increases with distance from the lidar in upstream direction) which was applied to correct the DEM that was compared with the reference DEM (resulting in Figure 3c).

The corrected set of DEMs were used to determine consecutive DoDs that were thresholded with a limit of detection using a 95%-confidence student t-test; Figure 3d gives the corresponding example for a non-consecutive grid. We quantified total detectable volumetric change in the river bed and associated uncertainty, assuming cell-based random error (Lane et al., 2003). Although a single scan position and relatively long distance scanning are not ideal considering errors related to shadowing and (potential) systematic error, these have been limited with the applied methodology and allow us to readily obtain data at a high temporal frequency.

3.4 2D Bedload transport rates

3.4.1 Morphological method

The morphological method (Ashmore & Church, 1998) provides a sediment budget approach to infer the minimum bedload transport rates that are required to account for total morphological change along a river section (Vericat et al., 2017). Here we applied the two-dimensional (2D) morphological method based on a framework first proposed by Lane et al. (1995) and described in detail by Antoniazza et al. (2019). This method gives additional insight into sediment origin and bedload routing within the river bed, allowing for more comprehensive sediment budgeting and the assessment of cross-channel morphological forcing.

We determined the local, grid cell based transport rates through considering bedload influx from adjacent cells and local topographic change as detected with consecutive lidar topographic surveys. Here we assume that all detected change can be associated with bedload transport. For any grid cell x, y, the two-dimensional volumetric form of the Exner equation is given by [2] (Antoniazza et al., 2019):

$$\left(\frac{\partial q_b^x}{\partial x}\right) + \left(\frac{\partial q_b^y}{\partial y}\right) + (1-\varepsilon) * \frac{\partial_{zxy}}{\partial_t} + \frac{\partial_{c_b}}{\partial_t} = 0 \qquad [2]$$

where q_b is the bedload transport in the x and y downstream and cross-stream directions respectively (the establishment of a bedload routing scheme will be discussed below), ε is the sediment porosity, z is elevation, t is time and c_b is the concentration per unit bed area of sediment in transport. Considering the total duration of effective flow per surveyed period ∂_t that led to the observed topographic change $\partial_{z_{xy}}$, we determined spatially-distributed, mean volumetric transport rates ($\partial_{c_b}/\partial_t$ = 0). These were converted to mass transport rates by assuming a sediment density of 2680 kg/m^3. A porosity of 0.18 was taken as typical for unsorted gravel and sediment (Carling & Reader, 1982). An important control on the sediment budget and routing is the sediment supplied to the reach at the upstream boundary, which could be accurately quantified based on the type and number of flow events that pass the intake during a given period (Figure 2d). We assumed that the impact of sediment input from tributaries on the morphological change is negligible and has little impact upon the studied reach.

3.4.2 2D Hydraulic modelling

To assess the 2D extent of the river bed where bedload transport occurs and to quantify the 2D bedload transport direction (x and y directions in Equation 1), 2D hydraulic simulations were performed using the open-source software BASEMENT v2.7 (http://www.basement.ethz.ch/). In BASEMENT, the finite volume method is applied based on the integral form of the shallow water equations (Vetsch et al., 2014) and a formulation for partially wetted cells (Begnudelli & Sanders, 2006) to reconcile these where flow depth is close to zero, such as at the wetting front during flow rise and the drying front during flow recession. The use of an explicit Euler scheme and an exact Riemann solver to integrate over time allow for the stable and accurate application in near-critical and super-critical flow conditions that are prominent in steep Alpine streams (Perona et al., 2009).

For each lidar scan we derived a 1 m resolution elevation grid (coarser than the 0.2 m DEM resolution for computational reasons) using the kriging approach mentioned earlier. This was the basis for the generation of a structured 2D mesh with the BASEmesh (v 1.4) plugin in QGIS. A spatially constant bed friction was used for model calibration of the reference grid (27 July), based on the propagation velocity of flushing events with different magnitudes over a dry river bed. We could relate these to a large number of events that were measured in the same period with in-stream stage measurements. A Manning's n value of 0.04 was found, which is lower than the value obtained by Antoniazza et al. (2019) for the same reach, yet commensurate given the higher resolution of the computational grid that was used in this case and therefore a reduced need to represent macro-roughness implicitly through a higher n value. Although sediment transport and morphological change simulations may be performed with BASEMENT, here we restricted the usage to determine steady-state flow conditions and applied these to address lidar-based observations of 2D morphological change.

3.4.3 2D Bedload routing

Sediment routing for the 2D morphological method (Antoniazza et al., 2019) was determined using the shear stress (τ) in the x and y direction resulting from local flow and the component of gravity along the local slope following Nelson and Smith (1989):

$$\tau_x = \rho_w g \frac{|u| u_x n^2}{d^{1/3}} + \tau_c \frac{\sin\alpha}{\sin\phi} \frac{s_x}{|s|} \quad [3a]$$

$$\tau_y = \rho_w g \frac{|u| u_y n^2}{d^{1/3}} + \tau_c \frac{\sin\alpha}{\sin\phi} \frac{s_y}{|s|} \quad [3b]$$

The first term of the right-hand side of [3a] and [3b] represents the bed shear stress due to the flow velocity magnitude ($|u|$) and direction ($u_{x,y}$), based on a Manning's n roughness formulation, where d is water depth in meters, water density ρ_w is 1000 kg/m^3 and gravity g is 9.81 m/s^2. The second term on the right-hand side of equations [3a] and [3b] describes the gravitational or topographic forcing of sediment routing, where τ_c is the critical shear stress for entrainment based on the Shields criterion, α is the arctan of slope $|s|$ which can be resolved into s_x and s_y, and ϕ is the bulk angle of repose of the sediment.

Derivation of the first term is based on the BASEMENT numerical simulations. For each period we determined a mean flow vector based on steady-state flow simulations of the initial and final river bed topography. The assumption of steady flow is reasonable considering that flushing involves very rapid flow rise and fall, and that these events are of relatively short duration. In Supporting Information S2 we address differences that may arise in 2D sediment routing when using flow routing based on the initial topography, as applied in Antoniazza et al. (2019) versus the final topography. This leads to a slightly adjusted distribution in bedload transport between adjacent channels (locally up to 20% of the total cross- sectional load) but not to large scale changes in bedload transport pathways. The combined wetted area of the flow calculations was used to delimit the morphological changes per period due to bedload transport which were also used in the further morphological analysis.

Similarly to Antoniazza et al. (2019), we used a generalised likelihood approach (Beven & Binley, 1992) to calibrate the sediment routing through minimizing total negative transport (sum of all inundated grid cells); here we implicitly assume that the error in transport results entirely from the error in bedload transport direction (and not from topographic measurements). We based this on 2000 simulations with randomly selected, plausible values of critical shear stress, bulk angle of repose and Manning's n, which address the relative contributions of the flow and gravity component of bed shear stress (see also Antoniazza et al. 2019). For all periods, effective values of τ_c = 150 N/m^2, ϕ = 30° and n=0.04 were found to be suitable, which may be expected in this setting and spatial resolution (see Supporting Information S2); the roughness value corresponds to that from the hydraulic simulations. Despite the use of a relatively simple routing model (based on steady state flow conditions, uniform roughness etc.) the resulting errors are limited. Areas of negative transport may amount up to c. 20% of the inundated area, which could also be attributed to suspended transport which we do consider here, while residual negative volumes are less than 5% of the total transport (see Supporting Information S2 for more detailed information).

3.5 Quantifying and assessing morphodynamics

Repeat, high frequency surveys of topographic change have been previously used to assess braided river morphodynamics (e.g. Lane et al., 2003; Milan et al., 2007; Williams et al., 2013). Here, we also used spatially-distributed, daily-based bedload transport rates to infer morphological activity that may not be recorded as a local river bed change (the DoDs), but rather can be deduced from surrounding morphological change. Besides quantifying the reach-based sediment budget from spatial changes in the river bed, we also: 1) considered cumulative absolute change and change frequency (number of periods with change) on a daily basis; noting that both are survey frequency dependent and do not include intermittent changes of scour and fill that lead to non-detectable change; and 2) quantified the spatial distribution of morphological age, that is the time since last reworking (Lane & Richards, 1997). Similarly, we assessed the temporal dynamics of bedload transport rates through transport frequency (number of periods with transport) and transport age (time since last transport).

To investigate the mechanisms that drive morphological change and sediment transport, we traced the transfer of sediment from the intake downstream through the reach to investigate the extent of the impact that the upstream flow and sediment supply had on river bed changes and sediment transport. For the whole reach, we quantified the influence of local relief on the subsequent morphological change, through correlating grid cell based morphological change with a normalized height index (topographic index TI) using major axis regression. For the topographic index, the inundated topography was scaled per cross-section x between 0, the deepest point, and 1, the highest point: $TI_{x,y} = (z_{x,y} - \min(z_y)_x)/(\max(z_y) - \min(z_y)_x)$. Similarly, we assessed the memory of the braided system, through correlating local morphological change in one period with that in the following period.

4 Results

4.1 Sediment budget

Over the whole period of investigation, from 6 June until 2 September, net erosion of the river bed took place, amounting to c. 2879 ±5 m^3 of detectable change. Erosion was dominant in June and July (-590 ±3 m^3) and in the second half of August (-3229 ±4 m^3). During the daily lidar surveys between 27 July and 13 August there was net aggradation of +940 ±5 m^3. On a daily basis, the total amounts of either erosion or deposition observed through river bed changes were on average a factor 3 larger than the net change; this factor ranges from less than 2 to as much as 10 for the flood of 10 August (Figure 4a). Despite the large scale erosion and sedimentation that took place throughout the river bed during the flood, the net effect was limited, amounting to not much more deposition than in the days preceding it. The 10th of August flood caused a marked shift from net sedimentation to net erosion in the days directly after the flood and later in August during which another flood occurred on the 14th of August. Similarly, a temporary response in terms of erosion was observed on 27 July, shortly after the flood of 24 July. Therefore, although the flood events were not necessarily erosive, there are indications that they may have impacted the river morphology making it susceptible to subsequent erosion during smaller flow events.

The mean rates of sedimentation and erosion during the investigation period varied much less than the associated volumes (Figure 4b). Most notably, the period that included the 10th of August flood showed similar rates as the days that preceded it, indicating the importance of the long flood duration and not necessarily high flow conditions in changing the river bed topography (Figure 2). However, we note that net changes are recorded in morphological change and that the actual, instantaneous rates may be much higher as intermittent scour and fill occurs.

The mean rate at which net daily morphological change occurred in the reach was related to the relative amount of upstream sediment supply and water yield (Figure 5; periods longer than 1 day are excluded to allow for comparable net changes). Where relative sediment input rates (sediment supply/water yield) drop below 0.02, this leads to a steeper trend in river bed degradation rates; typically when there were few normal gravel trap flushing events which are most efficient in terms of the water used to evacuate a volume of sediment. Here, there is no evidence that these erosion rates approached a maximum or were reduced due to river bed sorting and stabilization. Indeed, along the channel bottom no bed armouring was observed. On the other hand, increasing relative sediment input rates above 0.02 (generally a larger contribution of gravel trap flushing) leads to sedimentation, but the sedimentation rates increase more slowly as a function of the supply to yield ratio. This non-linear response to upstream forcing indicates changes in the efficiency with which sediment-laden flushing events could be transferred and hence changes in the river morphodynamics.

4.2 Morphological change

The observed variability in width-averaged bed level change was high both at specific locations between different events, particularly in the narrower stretches of the channel (upstream and downstream end), and for individual events along the reach (Figure 6). There was no apparent large scale morphological forcing that led to systematic bed changes along the river reach. A downstream recurring trend of net erosion and sedimentation could be distinguished in the period with the 10th of August flood which, particularly due to its long duration, caused large changes in river bed elevation.

The net morphological change for the period 27 July - 13 August was characterised by a distributed pattern of patches with net sedimentation and net erosion (Figure 7a). Local changes in both erosion and sedimentation ranged up to c. 2 m. The percentage of the bed that was reworked ranges from 25% upstream to nearly 75% of the active width downstream. The area of change comprised 48% net erosion with an average erosion depth of 0.35 m and 52% net sedimentation with an average thickness of 0.31 m. This indicates that erosional and deposition processes may lead to very similar yet opposite net changes, which may be expected in a bedload-dominated braided river system. Where the system is close to competence, it follows that patches of erosion and deposition are strongly coupled in space and related to the river bed morphology (see also Figure 6).

Temporal fluctuations in bed level between surveyed periods were locally very large as shown in the cumulative absolute change (Figure 7b). Although the absolute amounts depend strongly on survey frequency (the same applies for the change frequency in Figure 7c), hot-spots of temporal change were revealed whereas net change may be much smaller. In the upstream half of the reach these are local sites of temporary sediment storage which are repeatedly emptied and refilled (Figure 7b and c). In the downstream half of the reach these areas become less patchy and are more spread out over the width of the active river bed. A relatively large area of river bed was altered during the 10th of August flood (large area with age < 1 day in Figure 7d) which reworked earlier areas of erosion and sedimentation due to flushing events which were more local and channel-bound.

4.3 Sediment transport

Daily mean sediment transport rates in the period 27 July - 13 August are shown in Figure 8. On average, transport rates increased until the widening of the channel at c. 450 m distance, which was the result of the net erosion in this part of the reach (Figure 7a). At this location there is also a general decrease in slope and grain size in the reach (Bakker et al., 2018), from where there is gradual deposition in the downstream direction (Figure 8).

In general, the sediment input rates were larger than the fluctuations in transport rate down the reach which indicates the importance of upstream supply, which was for the most part transported through the reach. As with observations in Figure 5, low input rates tend to be associated with sediment transport increase along the reach (indicating erosion) and vice-versa, although this is not necessarily the case, and downstream fluctuations may be relatively large and local. The 10th of August flood appears to have contributed largely to the mean transport down the reach. Here we must note that there is a significant uncertainty in magnitude of the sediment supply and transport rates during this long, continuous flow period. Similar to width-averaged bed level change (Figure 6), sediment transport showed a large variability between different periods and in downstream direction (Figure 8). There appears to be no systematic upstream forcing of the local downstream sediment transport dynamics.

A significant proportion of the total estimated amount of bedload transport for the period 27 July - 13 August passed through a relatively narrow section of the channel, c. 5 m wide (Figure 9a; note the logarithmic scale). The main transport followed the right bank main channel between 400 and 800 m in the downstream direction. This is reflected in the observation that the largest morphological changes occur in the left channel which was abandoned (Figure 7b). Further downstream, from 1000 m, the bedload transport followed a remarkably straight path (Figure 9a). Uncertainties related to sediment routing may cause local, channel-based shifts in transport flux per period (see Supporting Information S2), but their limited magnitude and non-systematic nature have little impact on the longer term channelized character of bedload transport. We quantified total sediment transfer here as a volume, so it can be compared to the morphological change (Figure 7b), which reveals that transport may locally be orders of magnitude larger. Similarly, there are areas that frequently transferred sediment (Figure 9b) which appear to be inactive in terms of morphological change (Figure 7c). The age since last transport (Figure 9c) does not differ much from the morphological age (Figure 7d) due to the large-scale resetting of the age near the end of the surveyed period, during the 10th of August flood.

4.4 Morphological forcing of change

4.4.1 Local relief

We found that local relief has an impact on river bed change throughout the reach, where (net) sedimentation dominates change in the channel bottom and erosion dominates change at higher elevations within the wetted profile. This effect was particularly clear in the period with the 10th of August flood (Figure 10a). The influence of local relief upon morphological change was also present during intervals with sequences of flushing events, although the effect is minor (e.g. Figure 10b). Two observations can be made here which may not be directly evident. First, the range of (potential) morphological change was much higher for the flood than for the sequence of flushing events (and the maximum frequency values are lower). However, this did not yield a more scattered and weaker response, but rather a steeper and more significant (r-value) trend. Second, the duration of the flood event over which the channel bed evolves was also much longer than for the sequence of flushing events, the difference is nearly a factor 10 (Figure 2b). The influence of local relief was still stronger over the longer flow period, despite intermittent topographic change which may have altered the forcing. This was not the case when considering cumulative flushing events which showed a consistently weaker forcing of local relief (see Supporting Information S3), emphasizing the importance of the nature of the flow events for morphological response.

Figure 10c summarizes the influence of local relief, showing that the effect occurred throughout the investigation period. Large negative topographic gradients (the gradients of regression lines in plots a, b) and the overall significant and strong correlation (p <0.001) indicate the tendency to fill the lows (channel bottom) and to erode the highs (higher parts of the channel and bars) within the channel cross-section and are significant in nearly all cases. This provides a mechanism that allows these channels to rework their bed continually and to maintain a braided state, rather than to evolve to a single thread, stable morphology. Both erosion and sedimentation contributed to this mechanism, although the latter appears to be dominant (Figure 10c), and the effect was observed both in periods with net sedimentation and erosion (Figure 4a). In addition, the longer periods of change of 2 June until 27 July and 13 August until 2 September (both net erosion) show an effect very similar to the period with the 10th of August flood. This indicates that floods, despite their infrequent nature, may have a dominant impact on the long term, seasonal dynamics and may override daily effects from flushing events.

4.4.2 System memory

Besides being conditioned by channel bed topography, there is evidence that morphological change was also forced by earlier changes. The period including the 10th of August flood shows a weak dependency on earlier morphological change, in the form of a negative feedback (Figure 11a). In a period dominated by sediment-laden flushing events this effect was much clearer and strongly dominates the morphological response (Figure 11b). The data is strongly aligned with the negative feedback axis, the dashed line with equal quantities of opposite change. These observations are not significantly impacted by the orientation of the observed change, facing away or towards the lidar, or the absolute amount of observed change, indicating that the propagation of survey error into consecutive morphological changes does not play a prominent role here. The observed memory effect during flushing event sequences can be attributed to temporary sediment storage in the channel bottom, due to the high sediment loads and the abrupt on-off nature of these flows, which can be easily entrained during the next flushing event sequence. This illustrates the dynamic character of the braided reach with ample morphological change, but with a very small net change in sediment storage (see also Figure 4a).

Figure 11c generalises the results shown in Figures 11a and 11b. Over the total investigation period, in nearly all consecutive events, significant (p <0.001) and clear negative feedback was observed where a period of sedimentation is followed by erosion and vice versa. The memory effect of earlier morphological changes is less pronounced during periods with floods that largely respond to local relief (Figure 10c; 8 - 10 August and 13 August – 2 September) and apparently overwhelmed preceding sediment storage effects. The change gradient is negative throughout, despite variable upstream forcing (Figure 5), signifying a general autogenic mechanism that slows the rate of river bed aggradation or degradation.

5 Discussion

5.1 Spatial and temporal morphodynamics

In this study, we quantified the spatial and temporal morphodynamics of a braided Alpine river reach over different spatio-temporal scales and using a number of different metrics. Considering the spatial scale of the analysis, we found that net reach-based changes in the Borgne may be up to one order of magnitude smaller than total erosion and deposition that took place throughout the braided reach (Figure 4a). Similarly, when increasing the temporal resolution from the three week investigation period to the daily surveys, the total observed morphological change increases by as much as a factor two (Figure 7a vs. 7b). Because net change typically decays with time (Lindsay & Ashmore, 2002), we may expect even higher rates of change over even shorter timescales as observed by Antoniazza et al. (2019) at this site. Indeed, total transport volumes (Figure 9a) may locally be orders of magnitude higher than net morphological change (Figure 7a). These observations show that the frequency of resurvey is a crucial control on resolving temporal variability in morphological change (Lane et al., 1994; Lindsay & Ashmore, 2002; Milan et al., 2007). However, this temporal issue is countered by the spatial richness of the 2D morphological method (Antoniazza et al., 2019) or conceptually similar approaches (e.g. Kasprak et al.2018; Williams et al. 2016), which provide an effective way to interpret morphological change and to address braided river dynamics and processes. Here, the data illustrate the concentrated and efficient nature of bedload transport within a laterally relatively stable channel section (Figure 9a) while a much wider section of the studied reach is morphologically reworked (Figure 7a).

The temporal dynamics of the Borgne are directly affected by the short duration of flow events associated with the large-scale abstraction of water. The differences in scale, between high frequency small magnitude flushing events and low-frequency high-magnitude floods, also translate to a spatial signature in morphodynamics. This is reflected in distinct ages and perturbance frequencies observed in both morphological change and bedload transport (Figure 7c, 7d and Figure 9b and 9c), rather than a continuous spatial gradient. This may have important implications not only for the morphodynamic functioning of the system but also for vegetation and ecological succession (Gabbud & Lane, 2016). It also raises the question as to whether in more natural systems a continuum in surface reworking may be expected. Based on steady-state flume experiments, Wickert et al. (2013) found that the unreworked surface area decays exponentially in time. Under natural, unsteady forcing of flow and sediment input, however, thresholds in the system functioning, such as pavement breakup (Vericat et al., 2006) or above/below bankfull discharge (Bertoldi et al., 2010), may lead to a non-continuous reworking of the river bed in both space and time. Morphological change in proglacial braided rivers may be strongly impacted upon by meltwater floods, as Warburton (1992, 1994) found in the unregulated reach of the Borgne just upstream, or glacial outburst floods (Nicholas & Sambrook Smith, 2003). This indicates the importance of unsteady forcing of braided river morphodynamics which may have impacts that are not revealed in steady-state experiments.

5.2 Upstream and local forcing of morphodynamics

The spatial distribution of morphological change varied considerably in magnitude and direction throughout the braided reach of the Borgne (Figure 7a). River bed response to upstream sediment and water input during flushing events (external forcing) led to different rates of reach-scale morphological change (Figure 5): high sediment loads (gravel trap flushing) led to net aggradation at relatively low rates, while relatively low sediment loads (sand trap flushing and night-time flushing) led to degradation at much higher rates. The non-linearity in this response appears to be related to a (distinct) change in the way the river bed morphology conveys water and sediment, for instance due to changes in channel form and bed surface.

Although no large-scale spatial morphological forcing was evident along the reach (Figure 6), there was a notable effect of local relief that was found throughout the reach and investigation period (Figure 10). This is characterized by a tendency towards channel bottom deposition and erosion higher up in the channel or on the bars. The strongest effect was found in periods that contain floods, whose relatively long duration allow for more widespread and coherent morphological change to occur. In contrast, during flushing sequences, multiple relatively short phases of entrainment, transport and deposition led to a less apparent effect of local relief, also when these effects were accumulated over a longer period. Flow duration and competence here are insufficient to cause significant channel adjustment and the development of feedback mechanisms, typically where channel bottom sedimentation may induce bank erosion. The filling of lows and eroding of highs within the channel cross-section is a key mechanism that drives braided river dynamics through stimulating lateral channel migration and avulsion. Together with high sediment loads this mechanism allows high turnover rates to be maintained that prevent either the development of river bed armouring or the encroachment of vegetation, allowing the persistence of braiding processes (Harvey, 1991).

The morphodynamics of the river bed also showed negative auto-correlation, where morphological changes in one period were partly compensated in the next period, a memory effect which was particularly prominent in sequences of flushing events (Figure 11). Although the impacts of error recovery between DoDs cannot be eliminated in such an analysis, we found that this effect is driven by temporal dynamics of sediment availability in the main channel caused by the short duration and abrupt cessation of sediment-laden flushing events. Sediment that is deposited in the channel bottom during an event is only temporarily stored and can easily be entrained by the wave front in the following flushing event. This leads to a pulsed kinematic effect where sediment is transferred fairly efficiently through the system (Figure 9a). Mechanisms that affect changes in the bed surface and associated critical bed shear stress (Kirchner et al., 1990) may strengthen the observed memory effect. During channel bottom deposition, fine sediment preferentially fills the voids between the coarser grains, leading to a decrease in bed roughness and critical shear stress (Ferguson et al., 1989; Venditti et al., 2010), and hence facilitating erosion in a subsequent event (Johnson, 2016). Differences in flow conditions under which deposition in one event and entrainment in the following event occurs (Turowski et al., 2011) are not likely to play a role here due to the continuous high competence of the flows. In addition, low flows which may stabilize the river bed over time between higher flow events (Masteller & Finnegan, 2017; Reid et al., 1985) are absent due to flow abstraction.

Throughout the reach, it appears that there was a decreasing impact of flushing (memory effect) and increasing lateral dynamics (effect of local relief) in the downstream direction, where change was less concentrated in channel pockets and more widespread throughout the braided channel cross-section (Figure 7b). Whereas field-based studies have shown memory effects at measurement stations that provide bedload estimates at high temporal resolution (e.g. Turowski et al. (2011), in this study, we complement such work by showing the spatial extent and coherence of memory effects throughout a braided reach on a lower daily temporal resolution.

5.3 System dynamics driving morphological evolution

Over the whole period of investigation, June - September 2015, net river bed degradation occurred, which corresponds to the trend for the period 2010-2014 (Bakker et al., 2018). Erosion was observed in June - July and in the second half of August (Figure 4), both periods that experienced larger magnitude floods. Based on the daily surveys, however, we found sedimentation in the period with the 10^{th} of August flood and erosion in the days after the event (Figure 4), a response similar to that found at this site in 2013 (Antoniazza, 2015). It appears that there is a delayed transfer of sediment that was supplied to the reach by the flood and subsequently exported from the reach by a series of flushing events (Figure 8), which may be considered as a long-term memory effect. Note here that erosion occurs following flushing events which are designed to evacuate sediment from the sediment traps while using a minimal amount of water.

Floods may condition a morphological response where they typically leave behind channel bottom deposits (Figure 10a) that can be easily accessed by subsequent flushing events. In addition, grain size related mechanisms similar to those mentioned in relation to the memory effect, may also play a role here when fine sediment fractions may be accessed during the floods (Hoey and Sutherland, 1991; Lenzi et al., 2004) through for instance pavement break-up. Such effects are also expected to contribute to the change in response shown Figure 5, where all but one of the erosive periods (in)directly follow a flood event. Here, we want to stress that floods may have a phased impact on morphology and morphodynamics, which lasts longer than the duration of the event. Over the long term, these floods may cause critical changes in morphology that lead to subsequent river bed reworking and potential river bed degradation as found in this setting by Bakker et al. (2018).

Series of flushing events have been shown to be effective in the transfer of sediment (Figure 9a), despite their high sediment loads. The channelized nature of bedload transport previously found by Antoniazza et al. (2019) for a one day flushing sequence with low discharges, is maintained both at higher flows and over longer timescales. This relates to observations in less extreme and more natural settings such as just upstream in the unregulated pro-glacial reach of the Borgne where Warburton (1992) found narrow bands of transport, estimating up to an order magnitude change per meter cross-section. Elsewhere, Ashworth and Ferguson (1986) found that transport rates could be very efficient, even at low discharges, as a function of previous sediment delivery events. The efficient nature of sediment flushing in our case is reflected in the relatively low aggradation rates as shown in Figure 5, but also on the longer timescale. For the period 1959-2014, Bakker et al. (2018) show that flow capacity was still sufficient to export the majority (> 75%) of the sediment delivered to the reach, despite the presence of large scale flow abstraction (c. 90%) for hydropower.

6 Conclusions

In this study, we investigated the morphodynamics of a well-constrained Alpine braided river reach through frequent (daily) lidar topographic surveys. We also used these to determine spatially-distributed mean bedload transport rates which allowed changes to be inferred that are not recorded in the local geomorphology. We could therefore characterize the spatial and temporal signature of the system dynamics. Although a relatively wide section of the river bed was reworked, bedload transport was highly concentrated and efficiently transported through a narrow channel thread. The temporal variability of frequent, regulated flushing events and occasional floods translated into a non-continuous spatial reworking of the river bed with implications for morphological and ecological development. Although the impact of human regulation is evident in this setting, we argue that similar effects may result in more natural settings as a result of non-linear morphological response to external forcing, particularly associated with high magnitude flow events.

Non-linear morphological response to upstream sediment supply was observed for sequences of sediment-laden flushing events: flushing events with relatively low sediment loads led to high erosion rates, while events with relatively high sediment loads led to lower rates of sedimentation. The spatial distribution of bedload transport and local morphological change varied strongly within the braided reach and between successive flushing event sequences. Local morphological change was driven to a large extent by two effects that are found throughout the investigation period, regardless whether there was net aggradation or degradation. First, local relief led to the preferential filling of lower areas within the channel cross-section and erosion of higher areas. This effect was most prominent in the response to long duration floods and stimulates lateral channel instability (as opposed to the erosion of lows and filling of highs which would lead to vertical incision) that allows braided morphodynamics to be maintained. Second, system memory was present in the form of a negative feedback in bed level change: erosion in one period was followed by aggradation of a similar magnitude in the following period and vice-versa. This effect was most prominent in sequences of flushing events and could be attributed to the temporary storage of high sediment loads and the abrupt on-off nature of flushing flows. Deposited sediment was readily entrained during subsequent events, which may be enhanced through temporal bed surface changes that facilitate erosion. Despite their high sediment loads, flushing events may therefore still efficiently evacuate sediment through sequential transport and play an important role in maintaining relatively low aggradation rates in a river that is heavily impacted upon by flow abstraction for hydropower. In a wider context, insights in the mechanisms of morphological response may also be relevant for similar flashy, albeit more natural, flood regimes, such as in ephemeral streams.

In general, the data reveal a crucial point for how we conceptualize braided river dynamics. The internal morphodynamics of the system, impacted upon by the effects of local relief (space) and system memory (time), condition their own response to external forcing by, in this case, sediment-laden flows. Thus, events with similar external forcing may lead to a different morphodynamic response and consequently sediment transfer. This point challenges simplistic notions regarding the equilibrium morphology and emphasizes the need to factor in historic evolution and morphodynamics in order to quantify and predict future system response.

Acknowledgments

Maarten Bakker was supported by the Swiss National Science Foundation, Synergia grant CRSII2_147689, awarded to Fritz Schlunegger, Stéphanie Girardclos, Stuart Lane, Jean-Luc Loizeau and Peter Molnar. We would like to thank Grande Dixence SA, Alpiq, and Hydro Exploitation for providing discharge data and Chrystelle Gabbud for field support with the lidar surveys. We would also like to thank Editor John Buffington, Associate Editor Brett Eaton, Murray Hicks, Jon Tunnicliffe and Alan Kasprak for their detailed and constructive comments which have led to the improvement of this manuscript. DEMs, thresholded DoDs and bedload transport grids (including accompanying readme-file) are available on the online Alpine database Ebibalpin: http://ebibalpin.unil.ch/document/Bakker_et_al_2019/. For any further information on the used data please contact Maarten Bakker (maartenbakker@yahoo.com) or Prof. Stuart Lane (stuart.lane@unil.ch).

References

Antoniazza, G. (2015). Morphological forcing of erosion and deposition patterns in a braided river revealed through an Alpine field laboratory. Master's thesis in Geography, University of Lausanne.

Antoniazza, G., Bakker, M. & Lane, S. N. (2019). Revisiting the morphological method in two-dimensions to quantify bed material transport in braided rivers. Accepted for publication in *Earth Surface Processes and Landforms*. doi: 10.1002/esp.4633

Ashmore, P. & Church, M. (1998). Sediment transport and river morphology: a paradigm for study. *Water Resources Publications LLC, Highlands Ranch, Colorado*, 115-148.

Ashmore, P. E. (1982). Laboratory modelling of gravel braided stream morphology. *Earth Surface Processes and Landforms, 7*(3), 201-225.

Ashmore, P. E. (1991). How do gravel-bed rivers braid? *Canadian Journal of Earth Sciences, 28*(3), 326-341. doi:10.1139/e91-030

Ashworth, P. J. & Ferguson, R. I. (1986). Interrelationships of Channel Processes, Changes and Sediments in a Proglacial Braided River. *Geografiska Annaler. Series A, Physical Geography*, 68(4), 361-371. doi: 10.2307/521527

Bakker, M., Costa, A., Silva, T. A., Stutenbecker, L., Girardclos, S., Loizeau, J. L., . . . Lane, S. N. (2018). Combined Flow Abstraction and Climate Change Impacts on an Aggrading Alpine River. *Water Resources Research, 54*(1), 223-242. doi:10.1002/2017WR021775

Begnudelli, L. & Sanders, B. F. (2006). Unstructured Grid Finite-Volume Algorithm for Shallow-Water Flow and Scalar Transport with Wetting and Drying. *Journal of Hydraulic Engineering, 132*(4), 371-384. doi:10.1061/(ASCE)0733-9429(2006)132:4(371)

Bertoldi, W., Zanoni, L. & Tubino, M. (2010). Assessment of morphological changes induced by flow and flood pulses in a gravel bed braided river: The Tagliamento River (Italy). *Geomorphology, 114*(3), 348-360. doi:10.1016/j.geomorph.2009.07.017

Beven, K. & Binley, A. (1992). The future of distributed models: Model calibration and uncertainty prediction. *Hydrological Processes, 6*(3), 279-298. doi:10.1002/hyp.3360060305

Bezinge, A., Clark, M., Gurnell, A. & Warburton, J. (1989). The management of sediment transported by glacial melt -water streams and its significance for the estimation of sediment yield. *Annals of Glaciology, 13*, 1-5. doi:10.1017/S0260305500007527

Carling, P. A. & Reader, N. A. (1982). Structure, composition and bulk properties of upland stream gravels. *Earth Surface Processes and Landforms, 7*(4), 349-365. doi:10.1002/esp.3290070407

Ferguson, R. (1993). Understanding braiding processes in gravel-bed rivers: progress and unsolved problems. *Geological Society, London, Special Publications, 75*(1), 73-87. doi:10.1144/GSL.SP.1993.075.01.03

Ferguson, R. I., Prestegaard, K. L. & Ashworth, P. J. (1989). Influence of sand on hydraulics and gravel transport in a braided gravel bed river. *Water Resources Research, 25*(4), 635-643. doi:10.1029/WR025i004p00635

Gabbud, C. & Lane, S. N. (2016). Ecosystem impacts of Alpine water intakes for hydropower: the challenge of sediment management. *Wiley Interdisciplinary Reviews: Water, 3*(1), 41-61. doi:10.1002/wat2.1124

Gabbud, C., Micheletti, N. & Lane, S. N. (2015). Lidar measurement of surface melt for a temperate Alpine glacier at the seasonal and hourly scales. *Journal of Glaciology, 61*(229), 963-974. doi:10.3189/2015JoG14J226

Gomez, B., Naff, R. L. & Hubbell, D. W. (1989). Temporal variations in bedload transport rates associated with the migration of bedforms. *Earth Surface Processes and Landforms, 14*(2), 135-156. doi:10.1002/esp.3290140205

Gurnell, A. (1983). Downstream channel adjustments in response to water abstraction for hydro-electric power generation from alpine glacial melt-water streams. *The Geographical Journal, 149*(3), 342-354. doi:10.2307/634009

Gurnell, A., Warburton, J. & Clark, M. (1988). A Comparison of the Sediment Transport and Yield Characteristics of Two Adjacent Glacier Basins, Val d' Herens, Switzerland. *IN: Sediment Budgets. IAHS Publication* (174).

Harvey, A. M. (1991). The influence of sediment supply on the channel morphology of upland streams: Howgill Fells, Northwest England. *Earth Surface Processes and Landforms, 16*(7), 675-684. doi:10.1002/esp.3290160711

Heritage, G. L., Milan, D. J., Large, A. R. G. & Fuller, I. C. (2009). Influence of survey strategy and interpolation model on DEM quality. *Geomorphology, 112*(3–4), 334-344. doi: 10.1016/j.geomorph.2009.06.024

Hoey, T. (1992). Temporal variations in bedload transport rates and sediment storage in gravel-bed rivers. *Progress in Physical Geography: Earth and Environment, 16*(3), 319-338. doi:10.1177/030913339201600303

Hoey, T. B. & Sutherland, A. J. (1991). Channel morphology and bedload pulses in braided rivers: a laboratory study. *Earth Surface Processes and Landforms, 16*(5), 447-462. doi:10.1002/esp.3290160506

Johnson, J. P. L. (2016). Gravel threshold of motion: a state function of sediment transport disequilibrium? *Earth Surf. Dynam., 4*(3), 685-703. doi:10.5194/esurf-4-685-2016

Kasprak, A., Brasington, J., Hafen, K., Williams, R. D. & Wheaton, J. M. (2018). Modelling braided river morphodynamics using a particle travel length framework. *Earth Surf. Dynam. Discuss., 2018*, 1-53. doi:10.5194/esurf-2018-17

Kirchner, J. W., Dietrich, W. E., Iseya, F. & Ikeda, H. (1990). The variability of critical shear stress, friction angle, and grain protrusion in water-worked sediments. *Sedimentology, 37*(4), 647-672. doi:10.1111/j.1365-3091.1990.tb00627.x

Lane, S. N., Bakker, M., Gabbud, C., Micheletti, N. & Saugy, J.-N. (2017). Sediment export, transient landscape response and catchment-scale connectivity following rapid climate warming and Alpine glacier recession. *Geomorphology, 277*, 210-227. doi:10.1016/j.geomorph.2016.02.015

Lane, S. N. & Richards, K. S. (1997). Linking river channel form and process: time, space and causality revisited. *Earth Surface Processes and Landforms, 22*(3), 249-260. doi:10.1002/(SICI)1096-9837(199703)22:3<249::AID-ESP752>3.0.CO;2-7

Lane, S. N., Richards, K. S. & Chandler, J. H. (1994). Developments in monitoring and modelling small-scale river bed topography. *Earth Surface Processes and Landforms, 19*(4), 349-368. doi:10.1002/esp.3290190406

Lane, S. N., Richards, K. S. & Chandler, J. H. (1995). Morphological Estimation of the Time-Integrated Bed Load Transport Rate. *Water Resources Research, 31*(3), 761-772. doi:10.1029/94WR01726

Lane, S. N., Richards, K. S. & Chandler, J. H. (1996). Discharge and sediment supply controls on erosion and deposition in a dynamic alluvial channel. *Geomorphology, 15*(1), 1-15. doi:10.1016/0169-555X(95)00113-J

Lane, S. N., Westaway, R. M. & Hicks, M.D. (2003). Estimation of erosion and deposition volumes in a large, gravel-bed, braided river using synoptic remote sensing. *Earth Surface Processes and Landforms, 28*(3), 249-271. doi:10.1002/esp.483

Lenzi, M., Mao, L. & Comiti, F. (2004). Magnitude-frequency analysis of bed load data in an Alpine boulder bed stream. *Water Resources Research, 40*(7). doi:10.1029/2003WR002961

Lindsay, J. B. & Ashmore, P. E. (2002). The effects of survey frequency on estimates of scour and fill in a braided river model. *Earth Surface Processes and Landforms, 27*(1), 27-43. doi:10.1002/esp.282

Masteller, C. & Finnegan, N. J. (2017). Interplay between grain protrusion and sediment entrainment in an experimental flume. *Journal of Geophysical Research: Earth Surface, 122*(1), 274-289. doi:10.1002/2016JF003943

Micheletti, N. & Lane, S. N. (2016). Water yield and sediment export in small, partially glaciated Alpine watersheds in a warming climate. *Water Resources Research, 52*(6), 4924-4943. doi:10.1002/2016WR018774

Milan, D. J., Heritage, G. L. & Hetherington, D. (2007). Application of a 3D laser scanner in the assessment of erosion and deposition volumes and channel change in a proglacial river. *Earth Surface Processes and Landforms, 32*(11), 1657-1674. doi:10.1002/esp.1592

Murray, A. B. & Paola, C. (1994). A cellular model of braided rivers. *Nature, 371*, 54. doi:10.1038/371054a0

Nelson, J. M. & Smith, J. D. (1989). Evolution and stability of erodible channel beds. *River meandering*, 321-377.

Nicholas, A. P. & Sambrook Smith, G. H. (2003). Relationships Between Flow Hydraulics, Sediment Supply, Bedload Transport and Channel Stability in the Proglacial Virkisa River, Iceland. *Geografiska Annaler: Series A, Physical Geography, 80*(2), 111-122. doi:10.1111/j.0435-3676.1998.00030.x

Park, C. (1980). The Grande Dixence hydro-electric scheme, Switzerland. *Geography*, 317-320.

Perona, P., Molnar, P., Savina, M. & Burlando, P. (2009). An observation-based stochastic model for sediment and vegetation dynamics in the floodplain of an Alpine braided river. *Water Resources Research, 45*(9), n/a-n/a. doi:10.1029/2008WR007550

Reid, I., Frostick, L. E. & Layman, J. T. (1985). The incidence and nature of bedload transport during flood flows in coarse-grained alluvial channels. *Earth Surface Processes and Landforms, 10*(1), 33-44. doi:10.1002/esp.3290100107

Riegl. (2015). *Rigel Laser Measurement Systems: RiSCAN PRO version: 2.1.1*. Horn, Austria.

Turowski, J. M., Badoux, A. & Rickenmann, D. (2011). Start and end of bedload transport in gravel-bed streams. *Geophysical Research Letters, 38*(4). doi: 10.1029/2010GL046558

Venditti, J. G., Dietrich, W. E., Nelson, P. A., Wydzga, M. A., Fadde, J. & Sklar, L. (2010). Mobilization of coarse surface layers in gravel-bedded rivers by finer gravel bed load. *Water Resources Research*, *46*(7), W07506. doi:10.1029/2009WR008329

Vericat, D., Batalla, R. J. & Garcia, C. (2006). Breakup and reestablishment of the armour layer in a large gravel-bed river below dams: The lower Ebro. *Geomorphology, 76*(1), 122-136. doi:10.1016/j.geomorph.2005.10.005

Vericat, D., Wheaton, J. M. & Brasington, J. (2017). Revisiting the Morphological Approach *Gravel-Bed Rivers* (pp. 121-158): John Wiley & Sons, Ltd. doi: 10.1002/9781118971437.ch5

Vetsch, D., Rousselot, P., Volz, C., Vonwiller, L., Peter, S., Ehrbar, D., . . . Veprek, R. (2014). System Manuals of BASEMENT, Version 2.4. Laboratory of Hydraulics, Glaciology and Hydrology (VAW). ETH Zurich. http://www.basement.ethz.ch

Warburton, J. (1992). Observations of bed load transport and channel bed changes in a proglacial mountain stream. *Arctic and & Alpine Research*, *24*(3), 195-203. doi:10.2307/1551657

Warburton, J. (1994). Channel change in relation to meltwater flooding, Bas Glacier d'Arolla, Switzerland. *Geomorphology, 11*(2), 141-149. doi:10.1016/0169-555X(94)90078-7

Wheaton, J. M., Brasington, J., Darby, S. E., Kasprak, A., Sear, D. & Vericat, D. (2013). Morphodynamic signatures of braiding mechanisms as expressed through change in sediment storage in a gravel-bed river. *Journal of Geophysical Research: Earth Surface, 118*(2), 759-779. doi:10.1002/jgrf.20060

Wickert, A. D., Martin, J. M., Tal, M., Kim, W., Sheets, B. & Paola, C. (2013). River channel lateral mobility: metrics, time scales, and controls. *Journal of Geophysical Research: Earth Surface, 118*(2), 396-412. doi:10.1029/2012JF002386

Williams, R. D., Brasington, J., Vericat, D. & Hicks, D. M. (2013). Hyperscale terrain modelling of braided rivers: fusing mobile terrestrial laser scanning and optical bathymetric mapping. *Earth Surface Processes and Landforms, 39*(2), 167-183. doi:10.1002/esp.3437

Williams, R. D., Measures, R., Hicks, D. M. & Brasington, J. (2016). Assessment of a numerical model to reproduce event-scale erosion and deposition distributions in a braided river. *Water Resources Research*, 52(8), 6621-6642. doi: 10.1002/2015WR018491

Zhang, Z. (1994). Iterative point matching for registration of free-form curves and surfaces. *International journal of computer vision*, *13*(2), 119-152. doi:10.1007/BF01427149

Tables

Table 1. Reach dimensions and hydraulic parameters. Gradient and surface grain size are based on Figure 2 in Bakker et al. (2018) which provides a longitudinal profile of the reach.

Length	Width	Elevation	Gradient	Grain size	Vegetation
1700 m	20-120 m	2090-1985 m	11-5% (concave profile)	D50: 55 - 2 mm D84: 120 - 5 mm (downstream fining)	none

Figure captions

Figure 1. Aerial photo of the Borgne d'Arolla headwater reach and upstream hydropower flow intake. On the right a photo insert of the laser scanner overseeing the investigated reach from the vantage point. a) Hillshade map of the reach and mouths of regulated tributaries Douves Blanches (DB) and Pièce. b) Local error in elevation measurements of the reach due to point cloud density from the laser scanner survey. Channel bed outline used in the analysis is indicated by a black line. X- and y-axes of a) and b) are given in meters.

Figure 2. Summary of flow events per surveyed period. a) Maximum and average river discharge estimated from flow intake data. b) Average flow event duration (typically sediment trap flushing) and total flow duration. c) Relative contributions of different types of flow events. d) Water yield (volume) and sediment supply to the investigated reach during flow events (dashed line due to uncertainty in upstream sediment input due to floods).

Figure 3. a) Uncorrected DEM of difference (DoD) showing morphological change smaller than 0.2 m in the river bed (channel bed outline indicated by white line) and the surrounding area. b) Correction grid for systematic error or 'banding' based on regression analysis. c) DoD corrected for systematic error. d) DoD with 95% probability thresholding. X- and y-axes are given in meters.

Figure 4. a) Sediment budget on daily basis: net sedimentation, net erosion and net change in the braided reach and b) associated mean rates of change during effective flow (that is the total duration without flow intake).

Figure 5. Mean rate of net volume change in the river bed as a function of the upstream input of sediment supply (including uncertainties in sediment load) and water yield, given as a supply/yield ratio. Colors indicate the relative amount of gravel trap flushing events with respect to the total number of flow events (see also Figure 2c). Regression lines are given for negative and positive net volume changes.

Figure 6. Width-averaged channel bed level change as a function of distance downstream. The bed level change is smoothed with a 50 m running filter, the general scale at which morphological forcing may be expected along the braided reach, on a daily basis for the period 27 July - 13 August.

Figure 7. a) Net morphological change in the period 27 July - 13 August (greater than the limit of detection that is spatially variable but on average c. 10 cm). b) Cumulative absolute change measured on daily basis. c) Surveyed frequency of significant change (greater than the limit of detection of c. 10 cm). d) Morphological age of the river bed in terms of flow duration (not actual time because flow is intermittent). X- and y-axes are given in meters.

Figure 8. Width-averaged sediment transport as a function of distance along the braided reach on a daily basis in the period 27 July - 13 August. Transport during the flood period 8-10 August (orange) and average transport (black) are shown with a dashed line due to uncertainties in upstream sediment input.

Figure 9. Sediment transport in the period 27 July - 13 August expressed as a) transport volume (m^3 per m cell width) – note the log-scale, b) transport frequency (number of survey periods with transport), and c) transport age, i.e. flow duration since last recorded transport phase. X- and y-axes are given in meters.

Figure 10. Local relief effect: distribution of morphological change (Δz, greater than the limit of detection of c. 10 cm) along the relative depth of the wetted profile (Topographic Index) for the periods a) 8 - 10 August flood and b) 4 - 5 August flushing event sequence. Note the difference in y-axis extent. Major axis regression lines describe total change, and deposition and erosion separately. c) Gradient of local relief effect, corresponding to the gradient of regression lines in a) and b), representing the influence of local relief on morphological change in the investigation period. The strength of the relation is depicted as point size, the larger the point the stronger the correlation, the r-value in a) and b). No point is shown when the relation is not significant (p <0.001).

Figure 11. Memory effect: distribution of morphological change (Δz, greater than the limit of detection of c. 10 cm) for the periods a) 8 - 10 August change (y-axis) in response to the change in 7 - 8 August (x-axis) and b) 4 - 5 August change in response to the change in 3 - 4 August. Note the difference in y-axis extent. Major axis regression lines describe total change, and deposition and erosion separately. The dashed line indicates perfect negative feedback. c) Gradient of memory effect, corresponding to the gradient of regression lines in a) and b), representing the impact of changes on subsequent changes for all consecutive periods in the investigation period. The strength of the relation is depicted as point size, the larger the point the stronger the correlation, the r-value in a) and b). No point is shown when the relation is not significant (p <0.001).

Figure 1.

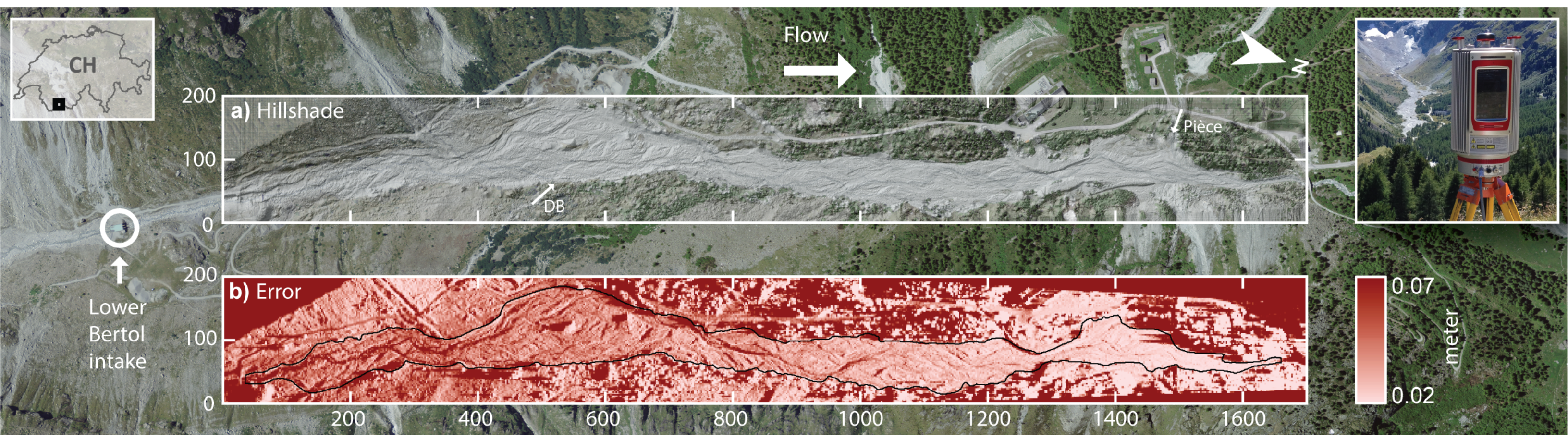
CH
Flow
N
a) Hillshade
Pièce
DB
200
100
0
b) Error
200
100
0
200
400
600
800
1000
1200
1400
1600
0.07
meter
0.02
Lower
Bertol
intake

Figure 2.

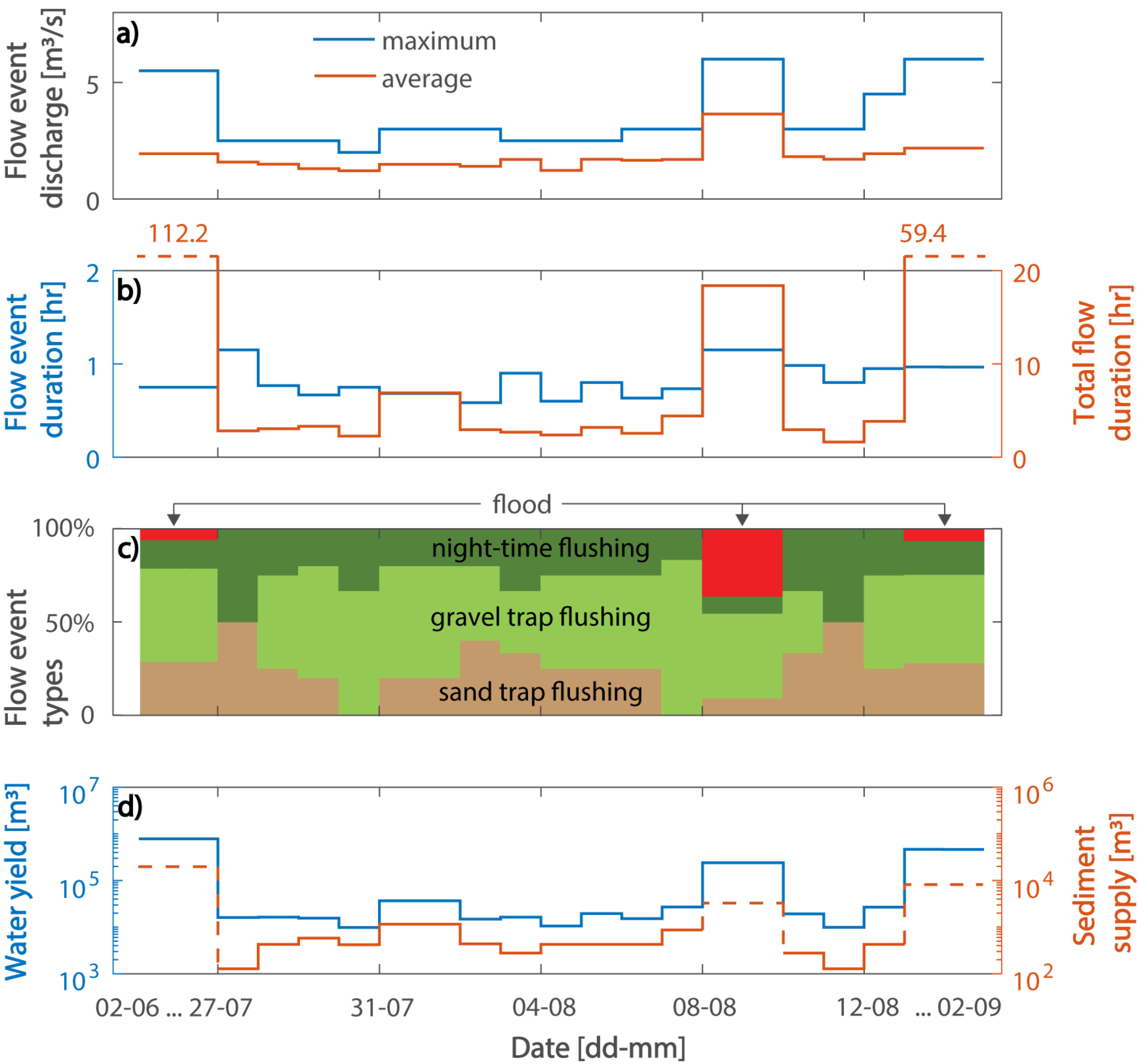

a)
maximum
average
Flow event discharge [m³/s]
5
0
112.2
59.4
b)
Flow event duration [hr]
Total flow duration [hr]
2
1
0
20
10
0
flood
100%
50%
0
c)
night-time flushing
gravel trap flushing
sand trap flushing
Flow event types
d)
Water yield [m³]
Sediment supply [m³]
02-06 ... 27-07
31-07
04-08
08-08
12-08
... 02-09
Date [dd-mm]

Figure 3.

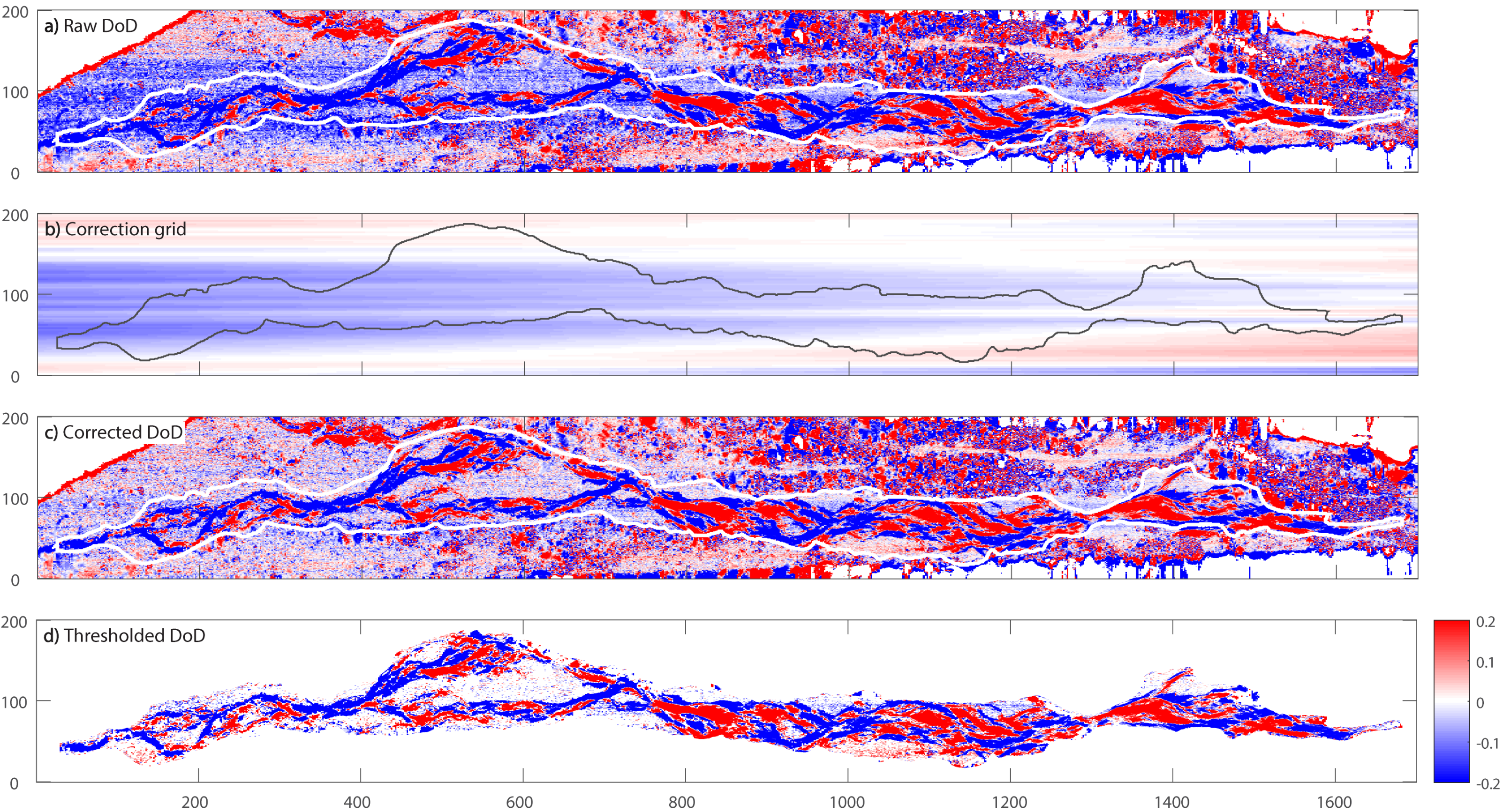

a) Raw DoD
b) Correction grid
c) Corrected DoD
d) Thresholded DoD
200
100
0
200
400
600
800
1000
1200
1400
1600
0.2
0.1
0
-0.1
-0.2
meter

Figure 4.

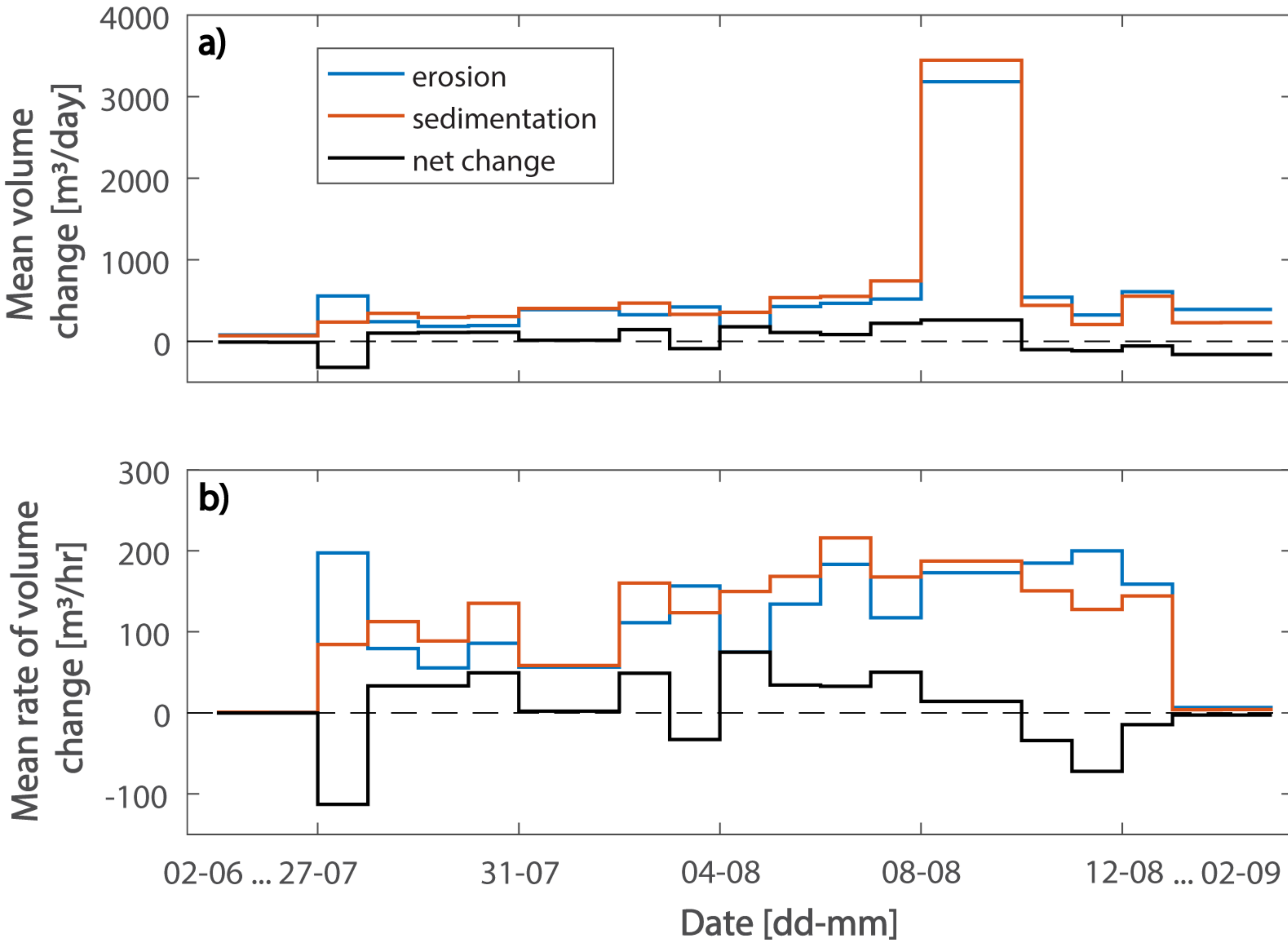

a)
b)
erosion
sedimentation
net change
Mean volume change [m³/day]
Mean rate of volume change [m³/hr]
4000
3000
2000
1000
0
300
200
100
0
-100
02-06 ... 27-07
31-07
04-08
08-08
12-08 ... 02-09
Date [dd-mm]

Figure 5.

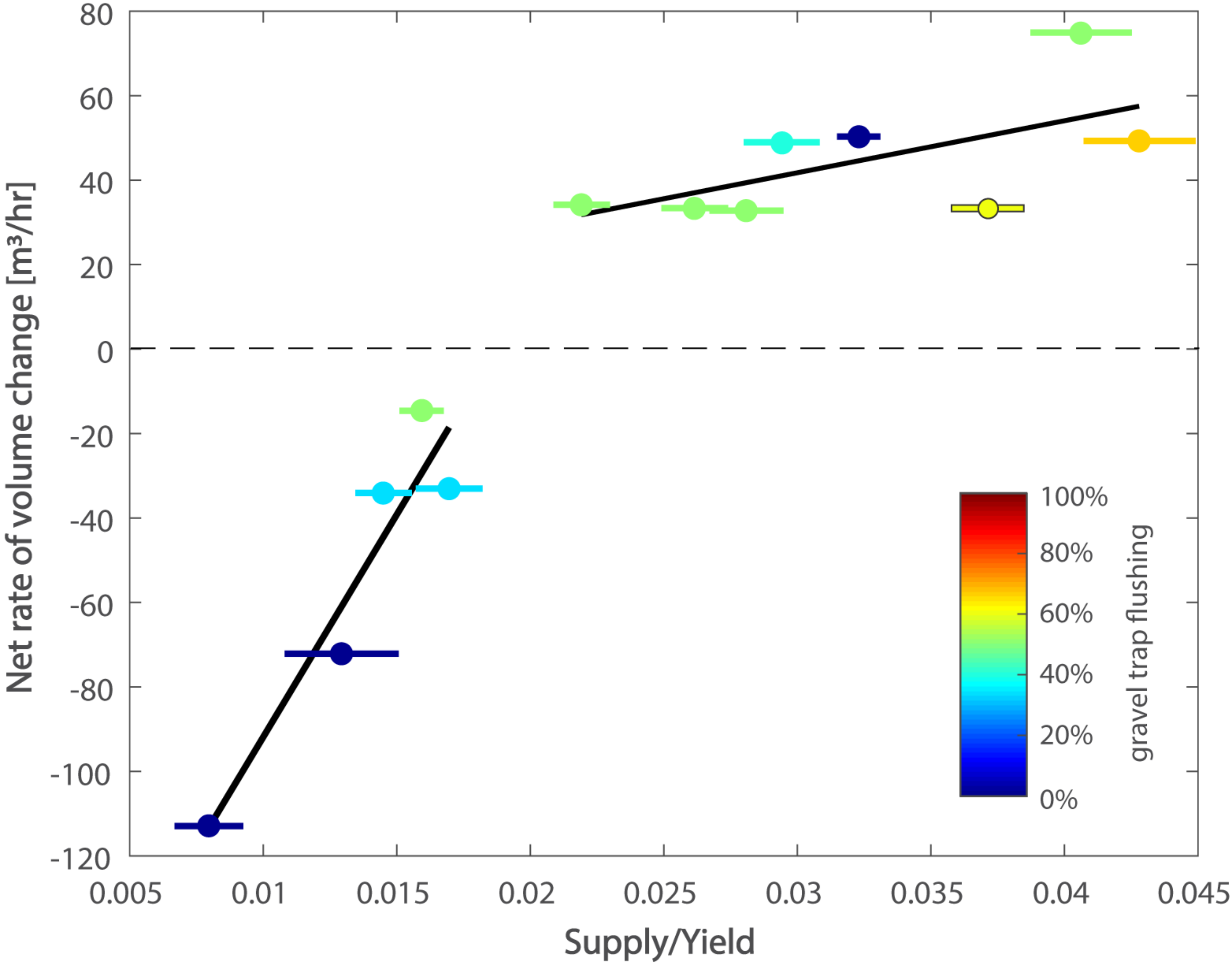

Net rate of volume change [m³/hr]
Supply/Yield
gravel trap flushing
100%
80%
60%
40%
20%
0%
80
60
40
20
0
-20
-40
-60
-80
-100
-120
0.005
0.01
0.015
0.02
0.025
0.03
0.035
0.04
0.045

Figure 6.

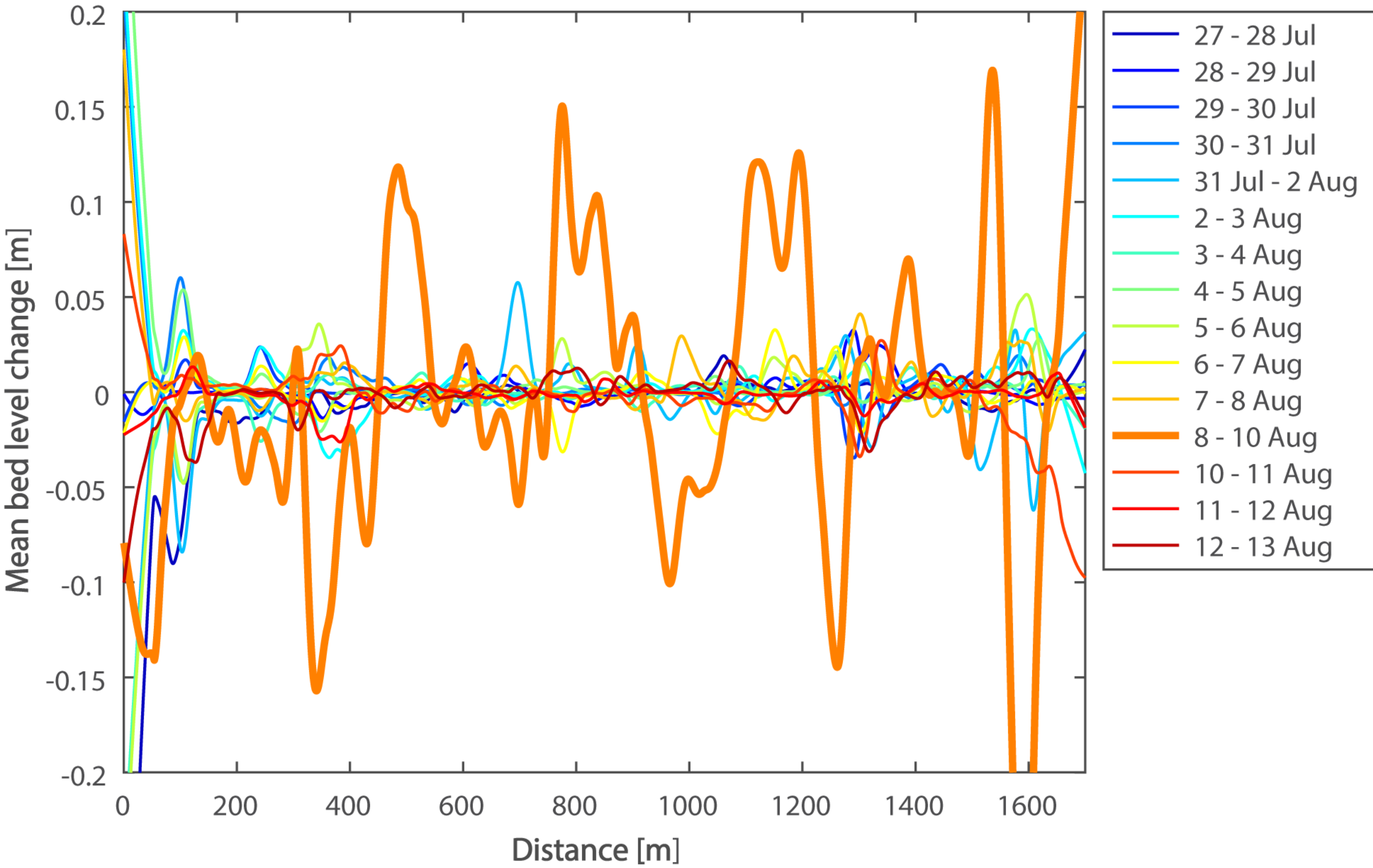

Mean bed level change [m]
0.2
0.15
0.1
0.05
0
-0.05
-0.1
-0.15
-0.2
0
200
400
600
800
1000
1200
1400
1600
Distance [m]
27 - 28 Jul
28 - 29 Jul
29 - 30 Jul
30 - 31 Jul
31 Jul - 2 Aug
2 - 3 Aug
3 - 4 Aug
4 - 5 Aug
5 - 6 Aug
6 - 7 Aug
7 - 8 Aug
8 - 10 Aug
10 - 11 Aug
11 - 12 Aug
12 - 13 Aug

Figure 7.

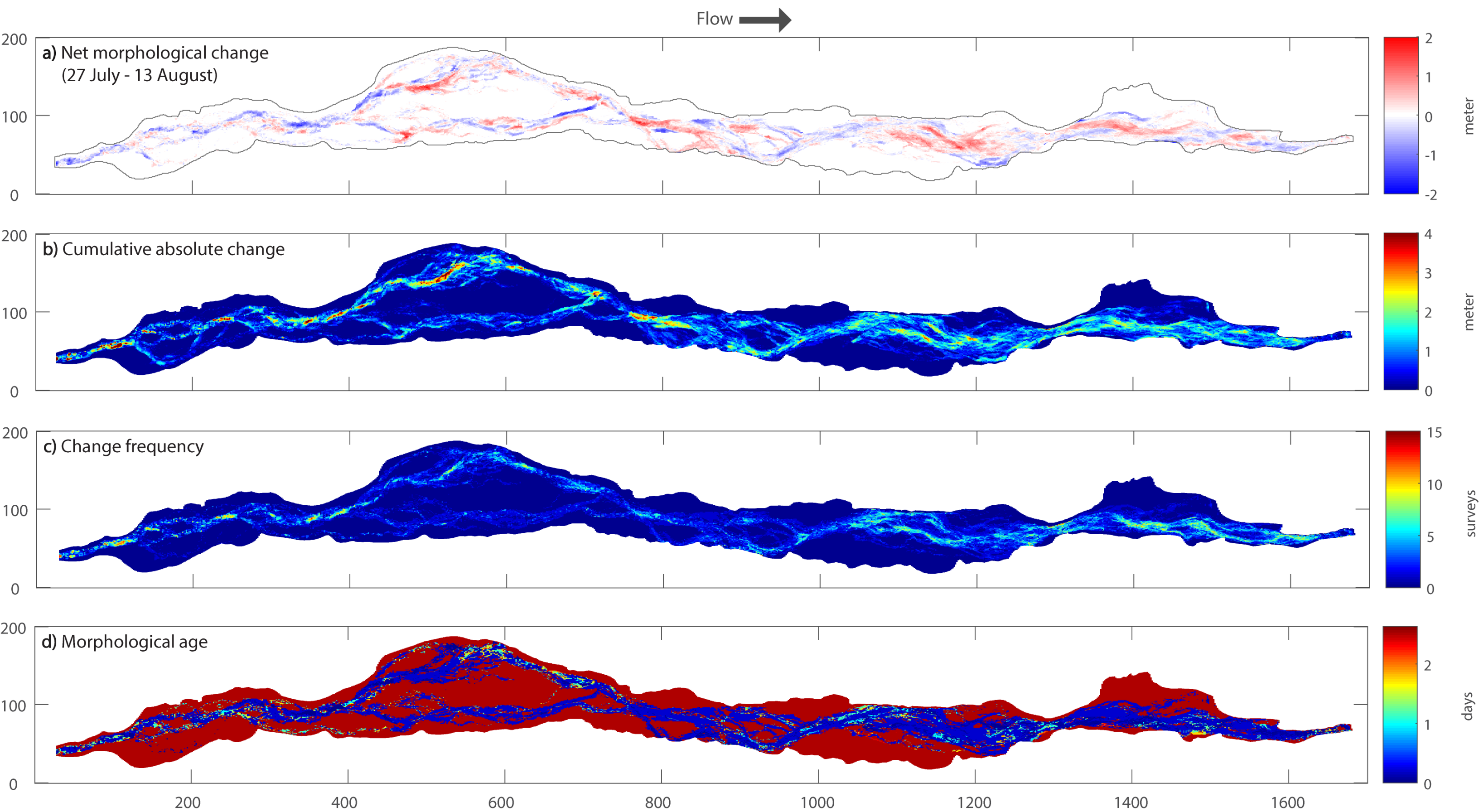
Flow
a) Net morphological change
(27 July - 13 August)
b) Cumulative absolute change
c) Change frequency
d) Morphological age
meter
meter
surveys
days
200
100
0
200
400
600
800
1000
1200
1400
1600

Figure 8.

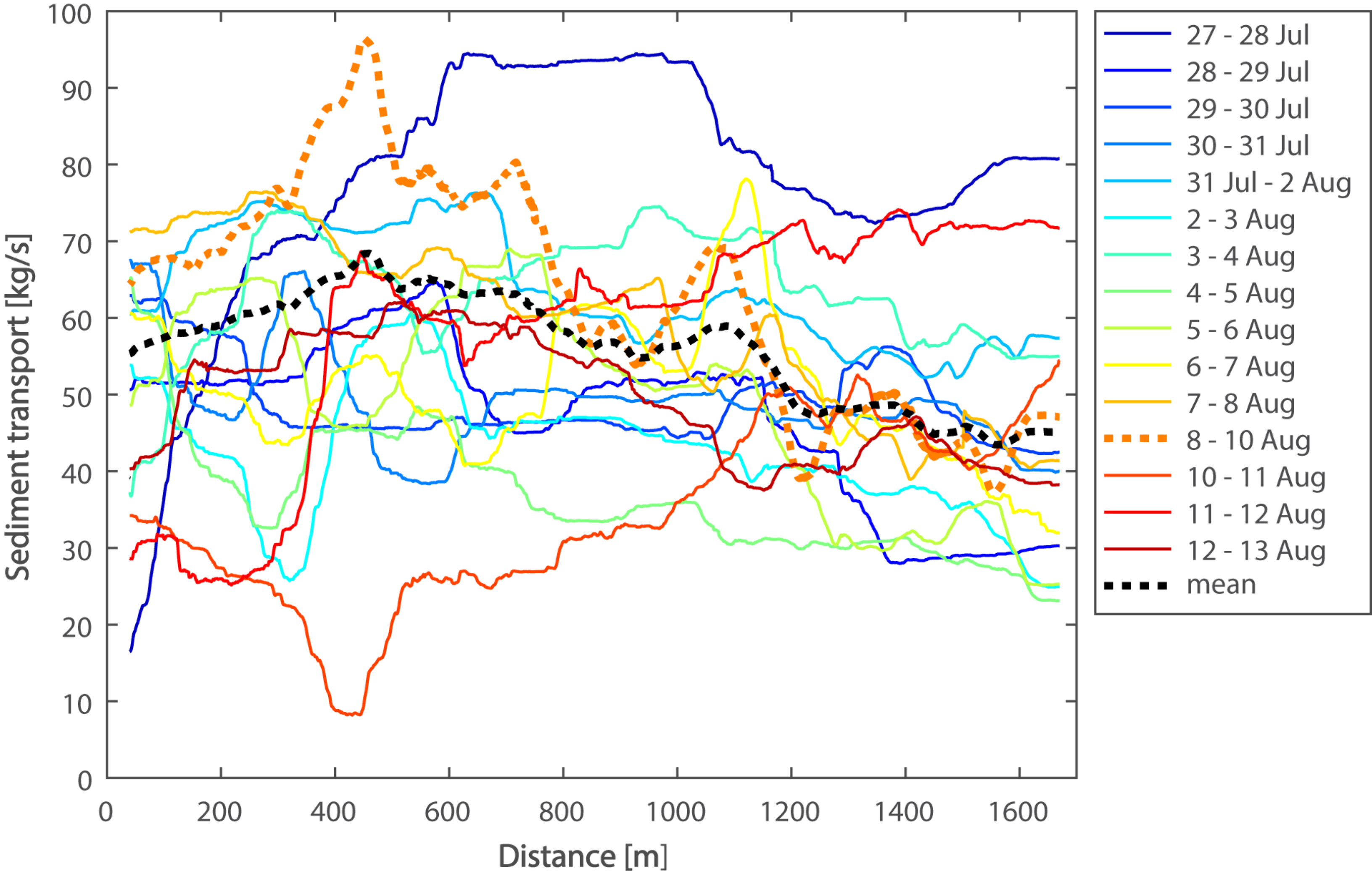
100
90
80
70
60
50
40
30
20
10
0
Sediment transport [kg/s]
0
200
400
600
800
1000
1200
1400
1600
Distance [m]
27 - 28 Jul
28 - 29 Jul
29 - 30 Jul
30 - 31 Jul
31 Jul - 2 Aug
2 - 3 Aug
3 - 4 Aug
4 - 5 Aug
5 - 6 Aug
6 - 7 Aug
7 - 8 Aug
8 - 10 Aug
10 - 11 Aug
11 - 12 Aug
12 - 13 Aug
mean

Figure 9.

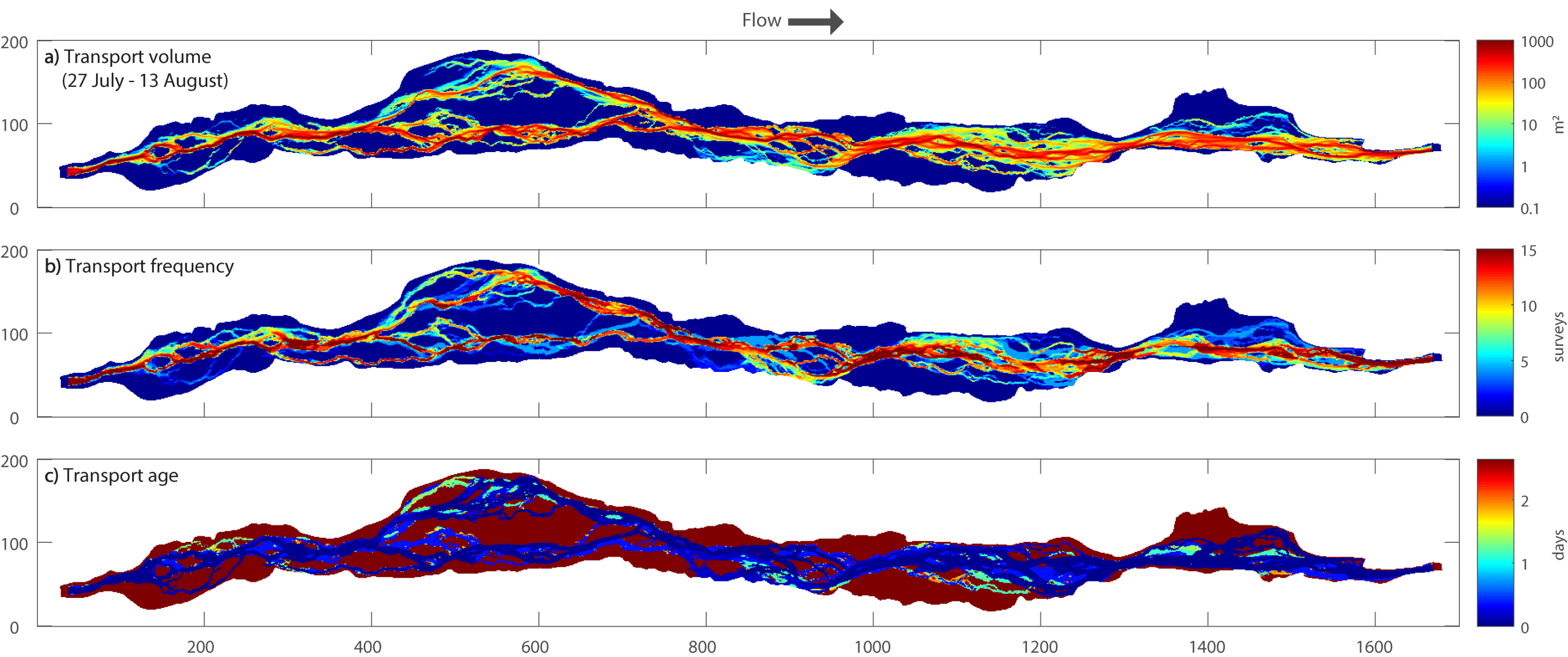

Flow
a) Transport volume
(27 July - 13 August)
b) Transport frequency
c) Transport age
200
100
0
200
400
600
800
1000
1200
1400
1600
1000
100
10
1
0.1
m²
15
10
5
0
surveys
2
1
0
days

Figure 10.

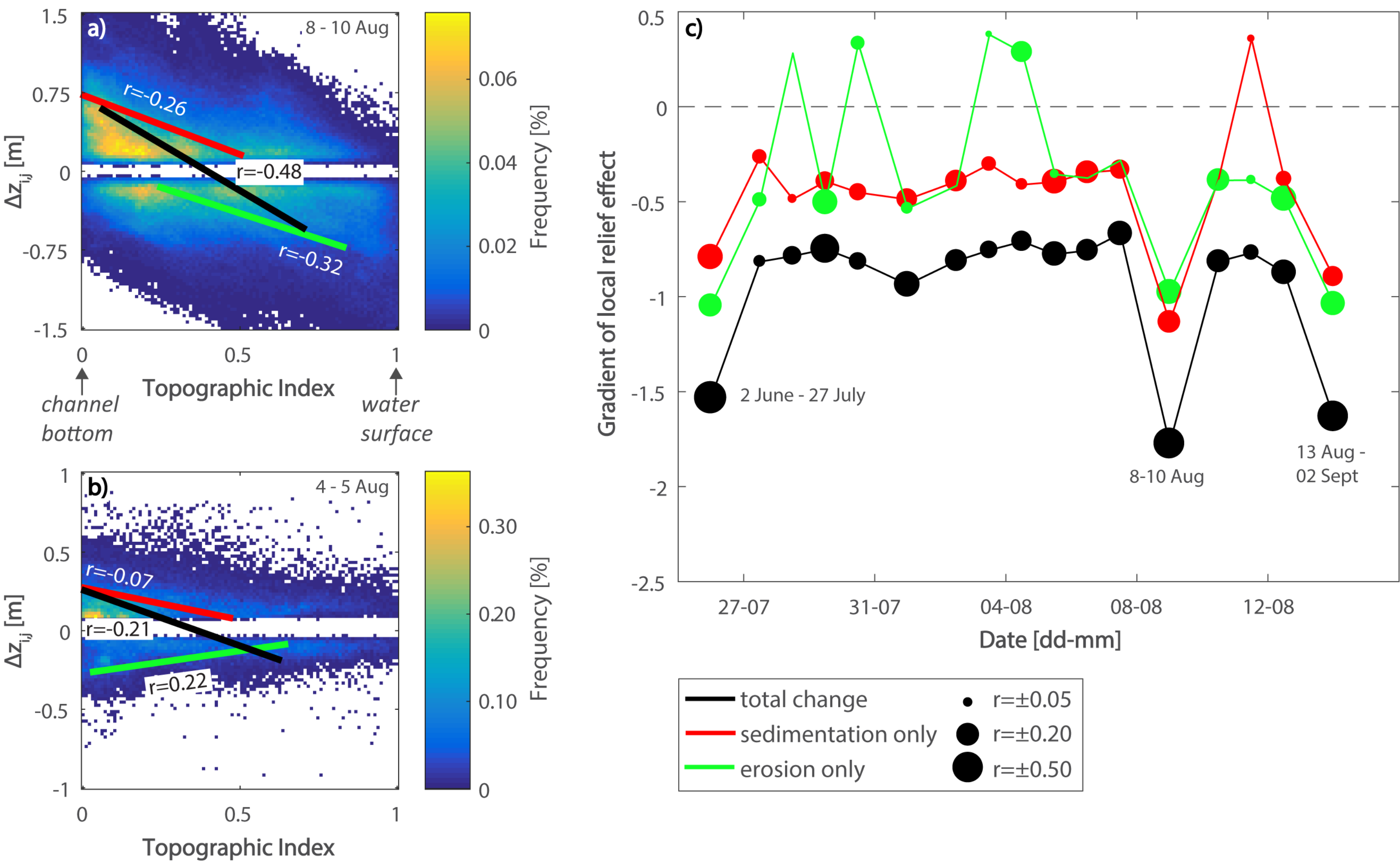

a)
8 - 10 Aug
r=-0.26
r=-0.48
r=-0.32
$\Delta z_{i,j}$ [m]
Frequency [%]
Topographic Index
channel bottom
water surface
b).
4 - 5 Aug
r=-0.07
r=-0.21
r=0.22
c)
Gradient of local relief effect
2 June - 27 July
8-10 Aug
13 Aug - 02 Sept
Date [dd-mm]
total change
sedimentation only
erosion only
r=±0.05
r=±0.20
r=±0.50

Figure 11.

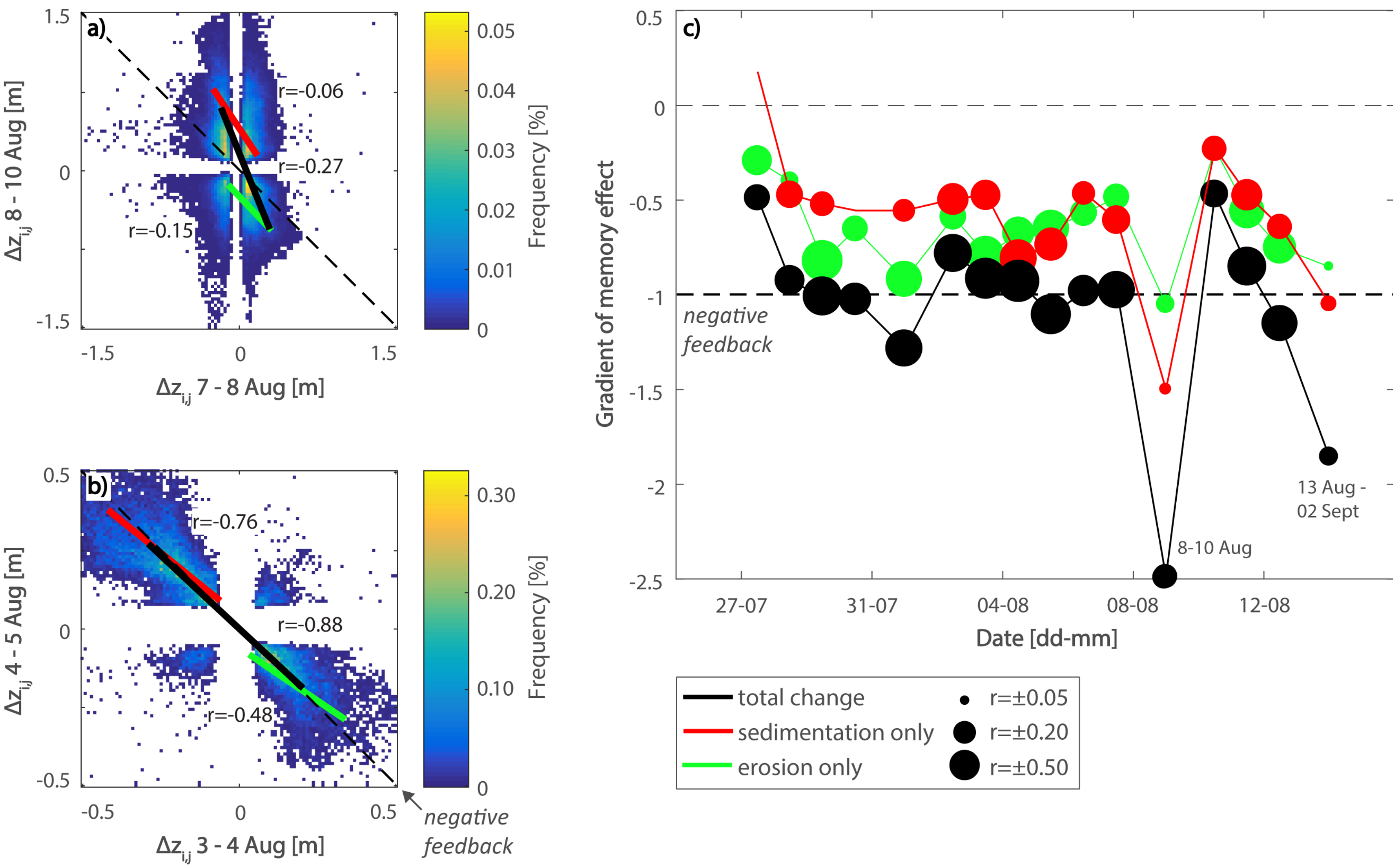
a)
r=-0.06
r=-0.27
r=-0.15
1.5
0
-1.5
Δz i,j 8 - 10 Aug [m]
Δz i,j 7 - 8 Aug [m]
0.05
0.04
0.03
0.02
0.01
0
Frequency [%]
b)
r=-0.76
r=-0.88
r=-0.48
0.5
-0.5
Δz i,j 4 - 5 Aug [m]
Δz i,j 3 - 4 Aug [m]
0.30
0.20
0.10
negative feedback
c)
Gradient of memory effect
0.5
-0.5
-1
-2
-2.5
negative feedback
8-10 Aug
13 Aug - 02 Sept
27-07
31-07
04-08
08-08
12-08
Date [dd-mm]
total change
sedimentation only
erosion only
r=±0.05
r=±0.20
r=±0.50